J Solid State Electrochem (2003) 7: 421–434
DOI 10.1007/s10008-002-0338-8

ORIGINAL PAPER

Gunnar Nurk · Jaanus Eskusson · Raivo Jaaniso
Enn Lust

Electrochemical properties of diamond-like carbon electrodes prepared by the pulsed laser deposition method

Received: 23 July 2002 / Accepted: 15 October 2002 / Published online: 27 November 2002

Abstract Diamond-like carbon electrodes (DLCEs) have been synthesized by the pulsed laser deposition method. The surface structure of the DLCEs has been studied by atomic force microscopy and the root-mean-square roughness has been established as $R_{ms} \geq 81$ Å. Electrochemical impedance spectroscopy and cyclic voltammetry data show that DLCEs are nearly ideally polarizable in the potential region $-0.4 < E < 1.1$ V (vs. Ag|AgCl|sat. KCl in H_2O) in 0.1 M $NaF + H_2O$ solution. Various equivalent circuits have been used for fitting the complex plane and Bode plots. A very good agreement between experimental and calculated Nyquist curves has been established if the charge transfer and double layer charging at the surface, intercalation of the H^+ and (or) Na^+ ions and solid phase diffusion inside the nanoparticle, as well as the effect of an insulating film at the surface (i.e. surrounding the nanoparticles), are taken into account.

Keywords Diamond-like carbon · Electrochemical double layer · Impedance · Pulsed laser deposition

Introduction

Diamond and diamond-like carbon electrodes (DLCEs) have been objects of very many fundamental and applied studies, but the electrochemical characteristics of the material are not very well established [1, 2, 3, 4, 5, 6, 7, 8, 9, 10, 11, 12, 13, 14, 15, 16, 17, 18, 19, 20, 21, 22, 23, 24, 25, 26, 27, 28, 29, 30, 31]. Diamond exhibits several remarkable properties of technological interest: it is very dense and extremely hard, has a large thermal conductivity and has free carriers with a high mobility [1, 2, 3, 4, 5, 17, 18, 19, 20, 21, 22, 23, 25, 26, 27, 28, 30, 31]. In its undoped form, diamond is an insulator with a band gap of ~5.5 eV. However, p-type conductivity and semi-metallic behaviour can be achieved by boron incorporation [1, 2, 3, 17, 25, 30, 31]. Highly doped diamond is also an interesting electrode material for fundamental electrochemistry studies, including the kinetics and mechanism of electron transfer processes. The excellent chemical inertness, combined with a low background current density and the large potential range between the onset of oxygen and hydrogen evolution, favour the use of diamond for the electroanalysis of a variety of electroactive species [6, 7, 8, 9, 17, 25]. Differently from many semiconductors and metals, diamond does not form a macroscopic oxide layer on its surface and it does not dissolve anodically (oxidize) or cathodically over a very wide potential region (~3.0 V) [9]. Theoretical calculations predict that the electronic properties of carbon forms will be variable over very wide limits. Interest in nanostructured carbon electrodes stems from their unique geometrical, mechanical, electronic and chemical properties. To date, most fundamental research on carbon nanotubes and carbon nanoporous materials has been focused on their growth mechanism [10, 11].

Electrochemical impedance studies show the very high capacitance values for polycrystalline diamond electrodes [1, 9, 12, 24, 25, 26]. Electrodes from good quality material with a faceted surface have a smaller interfacial capacitance than those from materials with polycrystalline (fractal or porous) surface morphology and surface regions, consisting of carbon in the sp^2 hybridization state [1, 8, 9, 12, 13, 14, 15, 16, 17, 28]. In some cases, the results indicated that the interfacial capacitance is determined by a majority carrier depletion layer and the capacitance versus voltage plot agrees with the Mott-Schottky relationship over a limited potential region [1, 2, 3, 12, 13, 14, 15, 16, 17, 25, 30, 31].

G. Nurk · J. Eskusson · E. Lust (✉)
Institute of Physical Chemistry,
University of Tartu, 2 Jakobi Street, 51014 Tartu, Estonia
E-mail: enn@chem.ut.ee

J. Eskusson · R. Jaaniso
Institute of Physics, Estonian Academy of Sciences,
142 Riia Street, 51014 Tartu Estonia

Usually, the highly boron-doped diamond (BDD) thin film electrodes were deposited on various conductive substrates, using microwave-assisted plasma-enhanced chemical vapor deposition and other similar methods [1, 2, 3, 4, 5, 6, 7, 8, 9, 10, 12, 13, 14, 15, 16, 17, 23, 25, 28]. In this work, we have prepared polycrystalline DLCEs using the pulsed laser deposition method [32], and established the impedance and cyclic voltammetry characteristics for the DLCE|*x*M NaF aqueous solution interface [10, 11].

Experimental

Deposition and characterization techniques of the DLCE

The scheme of the pulsed laser deposition (PLD) chamber of the DLCE is shown in Fig. 1 and an overview of the full computer-aided laser deposition system is given elsewhere [32]. The KrF eximer laser (ESTLA EXC-150/25) has been used to produce 25 ns pulses with a maximum energy of 250 mJ. The laser beam with a flux density of 8.5–9.0 J cm^{-2} was focused onto the liquid target [33, 34] at an angle of 45°. The target material was the vacuum pump oil "Santovac 5" (Edwards). The ablated material was deposited on the tip of a carbon cylinder with the dimensions 5×10 mm, which was surrounded on the lateral sides by a polystyrene film and additionally isolated by a Teflon holder [11, 35, 36, 37, 38]. The carbon substrates (CY-2500) were fixed with a stainless steel splint, which permitted easy exchange of the substrates and use of different target-substrate distances (a 40 mm distance was used in the present work).

Before being inserted into the chamber, the substrates were mechanically polished, cleaned with concentrated HF and $HClO_4$ [2], washed using MilliQ+ water and ethanol and thereafter rinsed with methanol.

The base pressure inside the deposition chamber was $\sim 10^{-6}$ mbar. Deposition was carried out at room temperature with the following laser parameters: pulse frequency, 10 Hz; spot area, ~ 1.5 mm^2; maximal number of pulses used, 1000. The thickness of the DLC layer was 30 ± 10 nm.

The Raman spectra (Fig. 2) were recorded with a spectrometer consisting of an Ar-ion laser (488 nm line), a double monochromator (SPEX 1402) and a cooled CCD camera (Andor, model DU420-BU). Topographical images of the film surfaces were measured with an Autoprobe CP (Park Scientific) atomic force microscope (AFM) (Fig. 3).

The electrical double layer impedance was measured using an Autolab PGSTAT 30 with a FRA 2 analyzer in the range of a.c. frequencies $0.01 < \nu < 10^4$ Hz with ± 5 mV modulation. NaF for preparing the solutions was purified by triple recrystallization from MilliQ+ water and treated in vacuum to dryness. NaF was calcined at 700 °C immediately prior to the preparation of the solutions. Pure Ar (99.9999%; from AGA) was bubbled for 1–2 h through the electrolyte before the submersion of the DLCE into the solution. The temperature was kept at 298 K. An AgCl|Ag (sat. KCl in H_2O) reference electrode was used and all the potentials are presented with respect to this electrode [11, 21, 22, 23, 24].

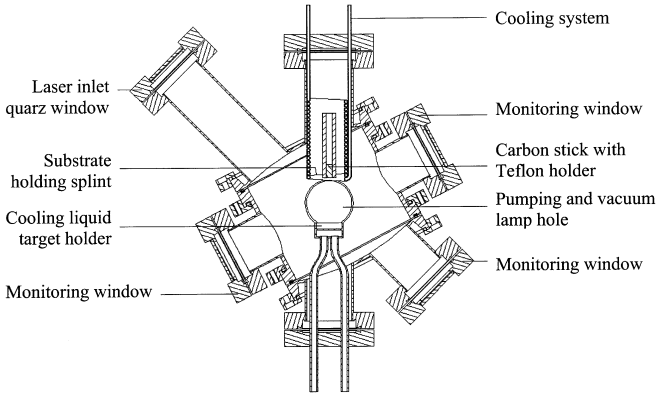

Fig. 1 Scheme of the pulsed laser deposition chamber

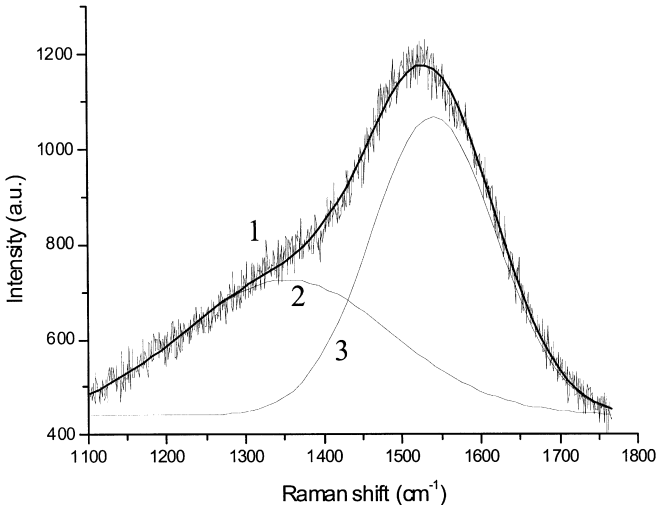

Fig. 2 Raman spectrum of a diamond-like carbon film deposited on a carbon substrate: *1*, total curve (*solid line*: fit); *2* and *3*, curves used for fitting the total Raman spectrum for the DLCE (explanations in text)

Results and discussion

Raman spectra (Fig. 2) of the samples, recorded in the range 1100–1800 cm^{-1} Raman shift wave numbers, consist of two broad bands peaking at 1353 cm^{-1} (D-band with the integral intensity I_D) and at 1541 cm^{-1} (G-band with the integral intensity I_G). The ratio of the integral intensities of the two bands is $I_D/I_G = 0.75$, and the widths of the spectral bands are 264 cm^{-1} and 160 cm^{-1}, respectively. Comparison of our results with the literature data [25, 28, 39, 40] shows that the shape of the spectrum in Fig. 2 is typical of amorphous diamond-like carbon films with a relatively high content of carbon in the sp^3 hybridization state. Based on results [39, 40] where the Raman spectra and electron energy loss spectra (EELS) were correlated for samples with different contents of carbon in the sp^3 hybridization state, it is possible to calculate that the ratio sp^3/sp^2 of the hybridization states is > 0.8 in our DLCE. However, taking into account the fact that the G-band in our samples is shifted toward smaller wave numbers (1541 cm^{-1}) compared with pure graphite (1580 cm^{-1}), the ratio of the sp^3/sp^2 hybridization states is probably somewhat higher than 0.8. This conclusion is in agreement with results [41, 42] where the shift of the G-band toward higher wave numbers has been explained by a higher content of carbon in the sp^2 valence state in DLCE samples.

AFM images of the carbon substrate (CY-2500) surface and DLC coatings were also measured in contact-mode regime and the results are shown in Fig. 3. The root-mean-square roughness (R_{ms}) values of these surfaces (determined from 1×1 μm DLCE areas) were 41 Å and 68 Å, respectively. Consequently, the roughness of DLC films is higher compared with the initial surfaces of the carbon substrates, and DLC particles have an average size of about 0.1 μm.

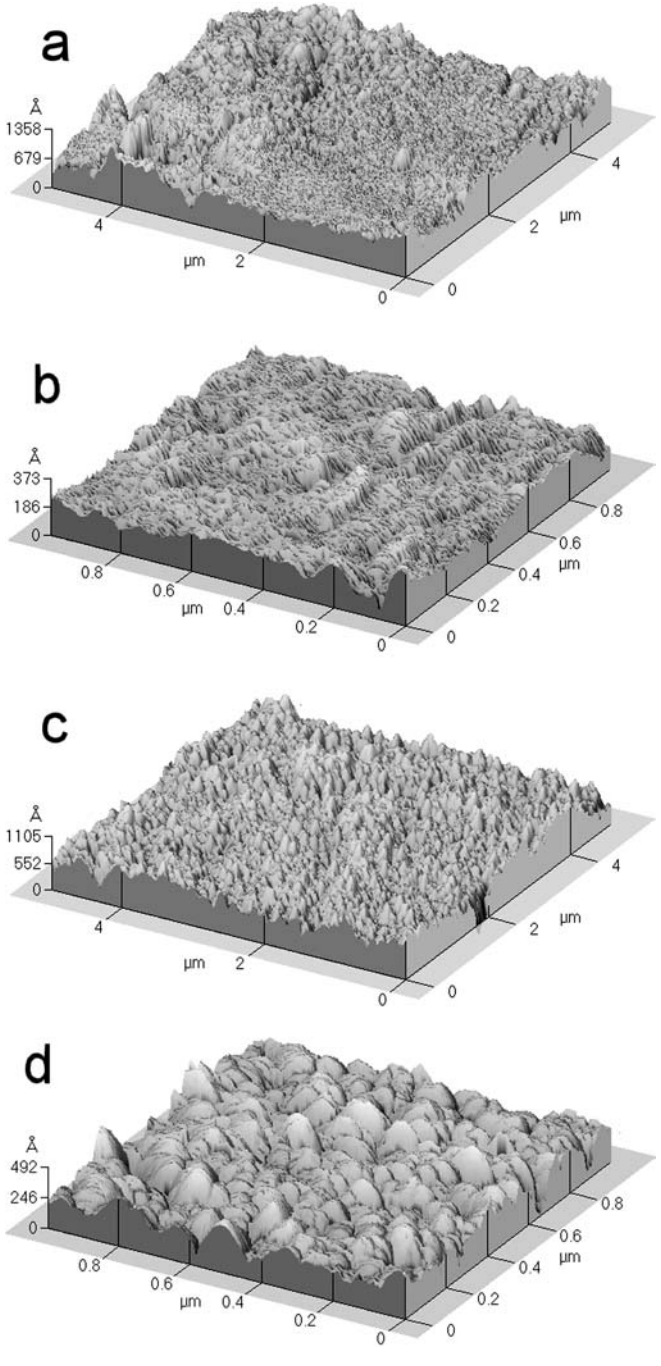

Fig. 3 AFM images of carbon substrates (**a** and **b**) and DLC films grown on the same substrates (**c** and **d**). The image areas are 5×5 μm (**a**, **c**) or 1×1 μm (**b**, **d**)

Results of electrochemical studies

Cyclic voltammograms

The CVs shown in Fig. 4a indicate that in the potential region $-0.4 < E < 1.0$ V [vs. AgCl|Ag (sat. KCl in H_2O)] the current density values are low and depend slightly on

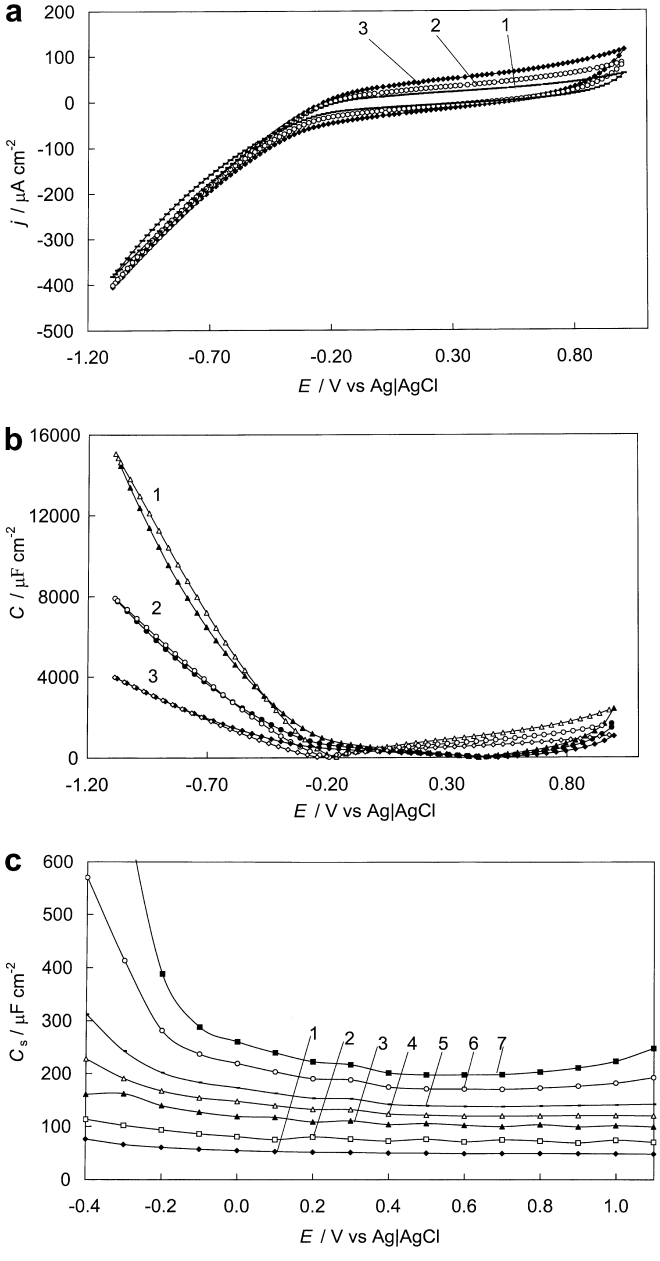

Fig. 4 **a** Current density vs. electrode potential curves and **b** differential capacitance vs. electrode potential curves (calculated from j vs. E curves; *open symbols*: potential scan toward less negative potentials; *filled symbols*: potential scan toward more negative potentials) for the DLCE in 0.001 M NaF solution at different potential scan rates (mV s^{-1}): 25 (*1*), 50 (*2*) and 100 (*3*). **c** Differential series capacitance C_s vs. E curves obtained from Z'' vs. Z' curves at different a.c. frequencies (Hz): 10 (*1*), 5.2 (*2*), 2.0 (*3*), 1.0 (*4*), 0.52 (*5*), 0.19 (*6*) and 0.10 (*7*)

the potential scan rate and, thus, in this potential region there are no rapid faradaic processes at the DLCE|0.1 M NaF aqueous solution interface. At $E < -0.4$ V, a rapid reduction process begins at the DLCE|0.1 M NaF aqueous solution interface. The shape of the j vs. E curves is typical of carbon electrodes in the region $-0.4 < E < 1.0$ V [2, 10, 11] and the capacitance values, C (Fig. 4b), calculated from j vs. E plots ($C = j/v$, where $v = dE/dt$ is the electrode potential scan rate), are in reasonable agreement with the series capacitance values (C_s) obtained from the complex plane plots ($-Z''$ vs. Z', i.e. so-called Nyquist plots [43, 44, 45, 46, 47, 48, 49, 50, 51, 52, 53, 54]: $Z'' = (jC_s 2\pi v)^{-1}$; $j = \sqrt{-1}$) at a frequency $v \approx 0.1$ Hz (Fig. 4c). The values of C are practically independent of v in the potential region $-0.30 \leq E < 0.80$ V and, thus, this potential region corresponds to the region of nearly ideal polarizability of DLCEs [43, 44, 45, 46, 47, 48, 49, 50, 51, 52, 53, 54, 55, 56, 57, 58]. At $E < -0.40$ V, the capacitance values decrease with the increase of the potential scan rate (Fig. 4b) and this effect can be explained by the very high resistance (i.e. by the very high potential drop [10, 11] inside the carbon electrode material [59, 60, 61]). It should be noted that additional studies in less concentrated electrolyte solutions are required to give more detailed results.

Complex plane plots

The complex plane plots obtained at various fixed electrode potentials (E = const.; $-0.4 < E < 1.1$ V) and at different NaF concentrations, presented in Figs. 5a, 6a and 7a, indicate that the shape of the Z'' vs. Z' plots depends noticeably on E, i.e. on the surface charge density, σ, of the DLCE. At potentials $-0.4 < E < 1.2$ V [vs. AgCl|Ag (sat. KCl in H_2O)], a depressed semicircle in the high-frequency region and nearly so-called "capacitive" behaviour (i.e. finite length effects [10, 11, 53, 54, 55, 56, 57, 58]) in the low-frequency region ($v < 10$ Hz) are observed. Differently from the nanoporous carbon electrodes, there is no so-called microporous region with a slope of 45° in the region of moderate frequencies [10, 11, 24, 29, 44, 45, 46, 47, 48, 49, 50, 51, 52, 53, 54]. It can be seen that, in the nearly capacitive region ($v < 10$ Hz), the curvature of the Z'' vs. Z' plots increases noticeably with the negative surface charge density, but the width of the depressed semicircle observed at higher frequency ($v > 19$ Hz) is practically independent of E. Comparison of the results in Figs. 5a, 6a and 7a shows that, at higher frequencies, the width of the first semicircle, i.e. the total series resistance (probably the sum of charge transfer and the bulk electrolyte resistance), increases with the dilution of the electrolyte solution.

The influence of the partial charge transfer process increases with the negative polarization (Figs. 5a, 6a and 7a), and at $E \leq -0.4$ V [vs. Ag|AgCl (sat. KCl)] there are two depressed semicircles in the complex plane plot, which can be explained by the increase in influence of the

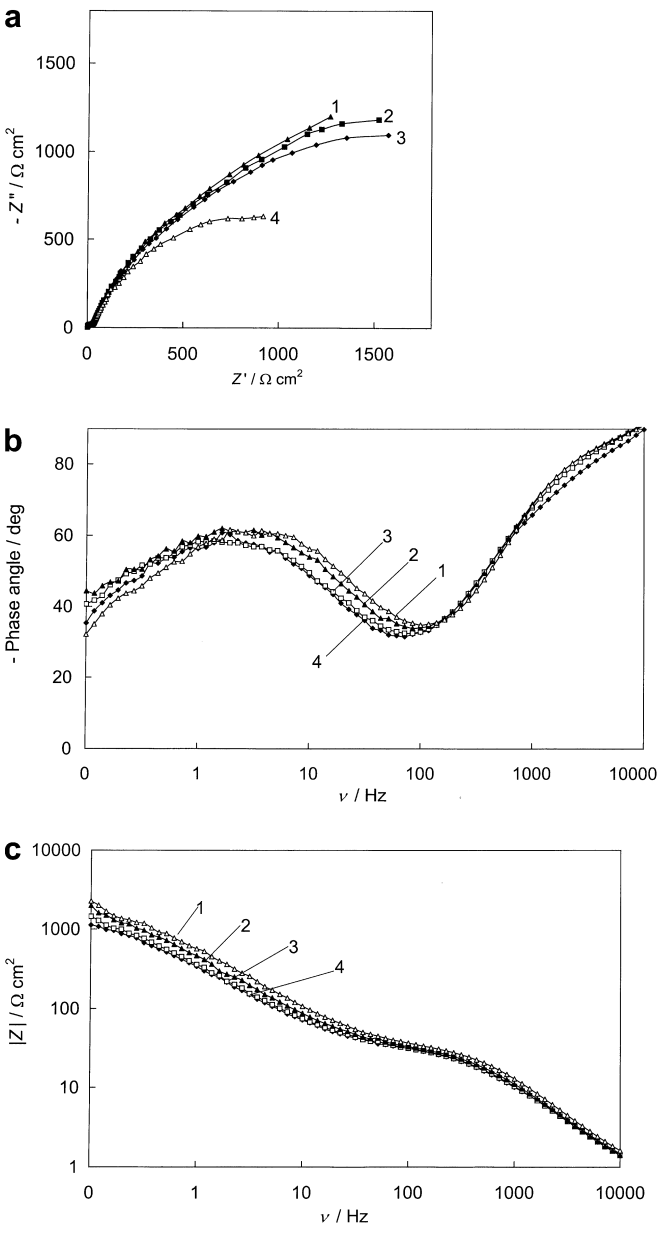

Fig. 5 **a** Complex plane plots [at electrode potentials (V): 0.2 (*1*), 0.6 (*2*), 1.1 (*3*) and –0.4 (*4*)]; **b** phase angle vs. a.c. frequency plots and **c** complex impedance vs. a.c. frequency plots [at electrode potentials (V): 1.1 (*1*), 0.2 (*2*), –0.2 (*3*) and –0.4 (*4*)] for the DLCE|0.1 M NaF + H_2O interface. Potentials have been given vs. Ag|AgCl (sat. KCl in H_2O) on all figures

parallel charge transfer resistance, i.e. by the decrease in resistance with the increase in rate of the cathodic faradaic processes (probably reduction of surface-active functional groups, reduction of Na^+ and H^+ or partial charge transfer process to the DLCE from the Na^+ ions during the adsorption step [10, 11]) at the negatively charged surface of the DLCE.

Analysis of complex plane plots shows that the frequency for the maximum of the depressed semicircle in the high-frequency region of the Z'' vs. Z' plots is practically independent of the electrolyte concentration

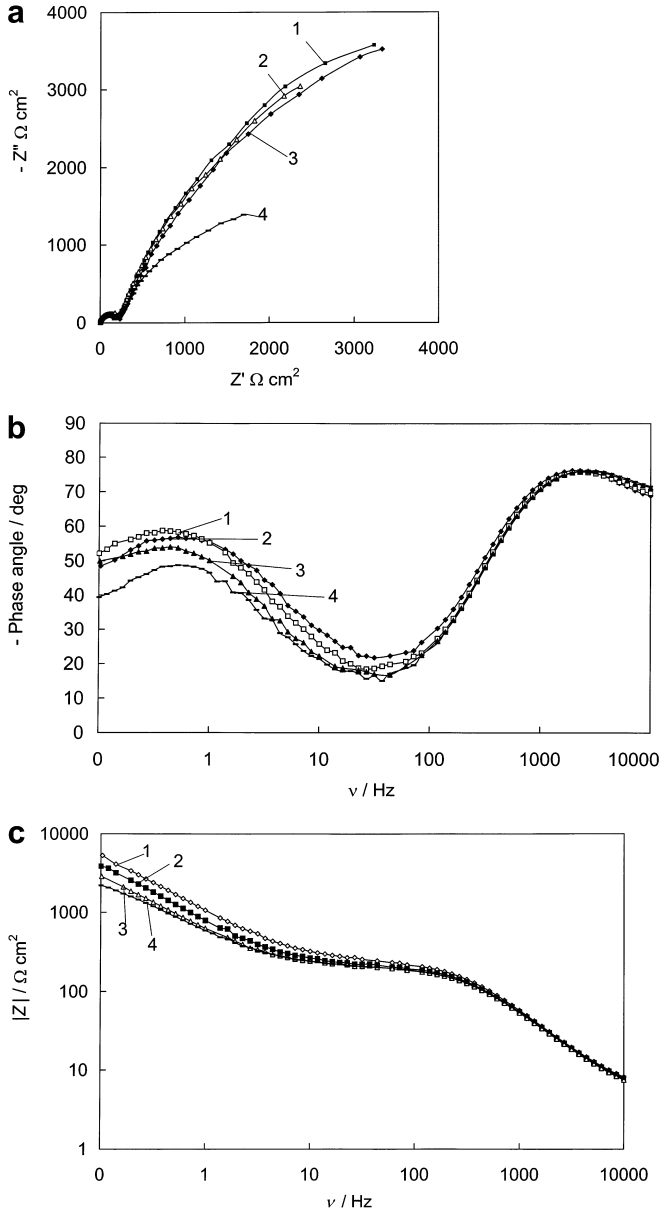

Fig. 6 **a** Complex plane plots [at electrode potentials (V): 0.6 (*1*), 0.2 (*2*), 1.1 (*3*) and –0.4 (*4*)]; **b** phase angle vs. a.c. frequency plots and **c** complex impedance vs. a.c. frequency plots [at electrode potentials (V): 1.1 (*1*), 0.2 (*2*), –0.2 (*3*) and –0.4 (*4*)] for the DLCE|0.01 M $NaF + H_2O$ interface

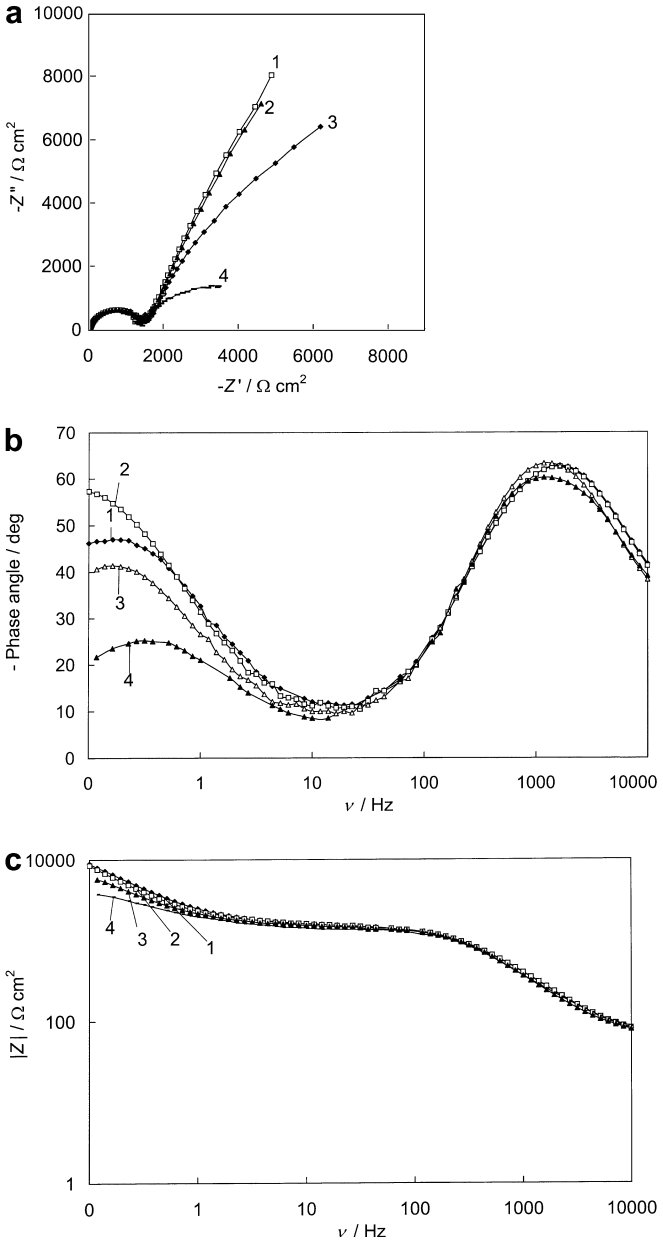

Fig. 7 **a** Complex plane plots [at electrode potentials (V): 0.6 (*1*), 0.2 (*2*), 1.1 (*3*) and –0.4 (*4*)]; **b** phase angle vs. a.c. frequency plots and **c** complex impedance vs. a.c. frequency plots [at electrode potentials (V): 1.1 (*1*), 0.2 (*2*), –0.2 (*3*) and –0.4 (*4*)] for the DLCE| 0.001 M $NaF + H_2O$ interface

as well as the electrode potential studied (if $E \geq -0.3$ V). Thus, the frequency $\omega_{max} = (\tau_{max})^{-1} = (R_b C_b)^{-1}$ (where τ_{max} is the characteristic relaxation time and R_b and C_b are the total resistance and total capacitance of the bulk electrolyte and electrode material, i.e. the capacitance of a "flat" electrode and the resistance of the high-frequency processes occurring on it) seems to be characteristic of the surface of the solid material|electric double layer interface. It is probably caused mainly by the space charge effects in the surface layer of the carbon material [45, 46, 47] and by the macroscopic Helmholtz layer capacitance characteristics for the flat electrode as well as by the diffuse (Gouy) layer characteristics. The value of R_b can be obtained from the Nyquist (Z'' vs. Z') plot, where the low-frequency and the high-frequency ends of the straight line coincide with series resistance R_s value [10, 11, 43, 44, 45, 46, 47, 48, 49, 50, 51, 52, 53, 54]. The frequency of the inflection point between the semicircle and the so-called capacitive (in our case nearly capacitive) region of the Z'' vs. Z' plots at $\nu < 10$ Hz is practically independent of c_{NaF} as well as of E, and probably characterizes the interplay of a.c. penetration depth λ and the macroscopic surface roughness characteristics of the DLCE [10, 11].

The Bode plots (i.e. the phase angle $|\delta|$ and complex impedance $|Z|$ vs. logν dependences) (Figs. 5, 6, 7, parts b and c) indicate that there is a minimum in the $|\delta|$ vs. logν curves ($|\delta| < 10$ for 1×10^{-3} M NaF) and, thus, there are no processes (faradaic) on the DLCE|NaF + H_2O interface with characteristic frequency values in this region of ν. At fixed electrolyte concentrations the values of $|Z|$ and $|\delta|$ do not depend on the potential if $\nu \geq 100$ Hz. For 0.01 M and 0.001 M electrolyte solutions, there is a maximum in the $|\delta|$ vs. logν curves with the value $|\delta| \geq 63°$, characteristic of the kinetically mixed process ($\delta = -45°$ for diffusion limitation and $\delta \approx -90°$ for pure capacitive behaviour [10, 11]). The absolute value of the phase angle $|\delta|$ and the frequency maximum increase with the electrolyte concentration. Thus, deviation of the DLCE|xM NaF + H_2O interface from the behaviour characteristic of the pure capacitance increases on dilution of the electrolyte.

At smaller frequencies (Figs. 5, 6, 7, parts b and c), the values of $|Z|$ and $|\delta|$ start to increase, and at $0.05 \leq \nu \leq 10$ Hz there is a maximum in the δ vs. logν plot with the value $|\delta| \geq 65°$ (for 1×10^{-1} M), which is mainly characteristic of the kinetically mixed limited process at the rough surfaces (adsorption and diffusion-limited stages in the interior of the electrolyte). The slope of the $|\delta|$ vs. logν dependence remarkably depends on c_{NaF} and the maximum values of $|\delta| \geq 45°$ for $c_{NaF} = 0.001$ M have been established only at very low frequencies ($\nu \leq 0.1$ Hz). This result is probably caused mainly by the interplay of the Debye screening length and surface roughness of the DLCE electrode [11, 36, 37, 38, 62, 63]. With the increase of the electrolyte concentration, the frequency of this frequency maximum, ν_{max}^{lf} (in the low-frequency region), shifts toward higher frequencies, i.e. toward smaller relaxation times $\left(\tau_{max}^{lf} = \left(\nu_{max}^{lf}\right)^{-1}\right)$. The values of $|\delta|$ are maximal at $E \approx 0.2$ V and the dependence of $|\delta|$ on c_{NaF} is more noticeable for more dilute solutions ($c_{NaF} \leq 1\times10^{-3}$ M).

In comparison with a nanoporous carbon electrode (NPCE), the low-frequency characteristic relaxation time, τ_{max}^{l}, is noticeably shorter for a DLCE than for a NPCE (approximately 10^3 times) [11]. The dependence of the series capacitance C_s [obtained from $Z' = (j2\pi\nu C_s)^{-1}$] and parallel capacitance C_p on $\omega^{1/2}$ (Fig. 8a) and C_s, C_p and R_p on logν are in a good agreement with the conclusion made above, and the coincidence of these dependences in the region $10 < \nu < 10{,}000$ Hz (Fig. 8b and c) indicates that there is no rapid faradaic charge transfer reactions at the DLCE|xM NaF + H_2O interface. The series capacitance values C_s decrease on dilution of the electrolyte; thus, weak adsorption of Na^+ cations on the DLCE is possible.

At $\nu \geq 1000$ Hz, the values of C_s and C_p are of the same order as the values obtained for the flat single-crystal Bi, Ag and Cd electrodes [35, 36, 37, 38]. Thus, in this region of ν where the a.c. penetration depth is small, the surface of the DLCE seems to be comparatively flat (the DLCE surface works as a flat surface). In the region

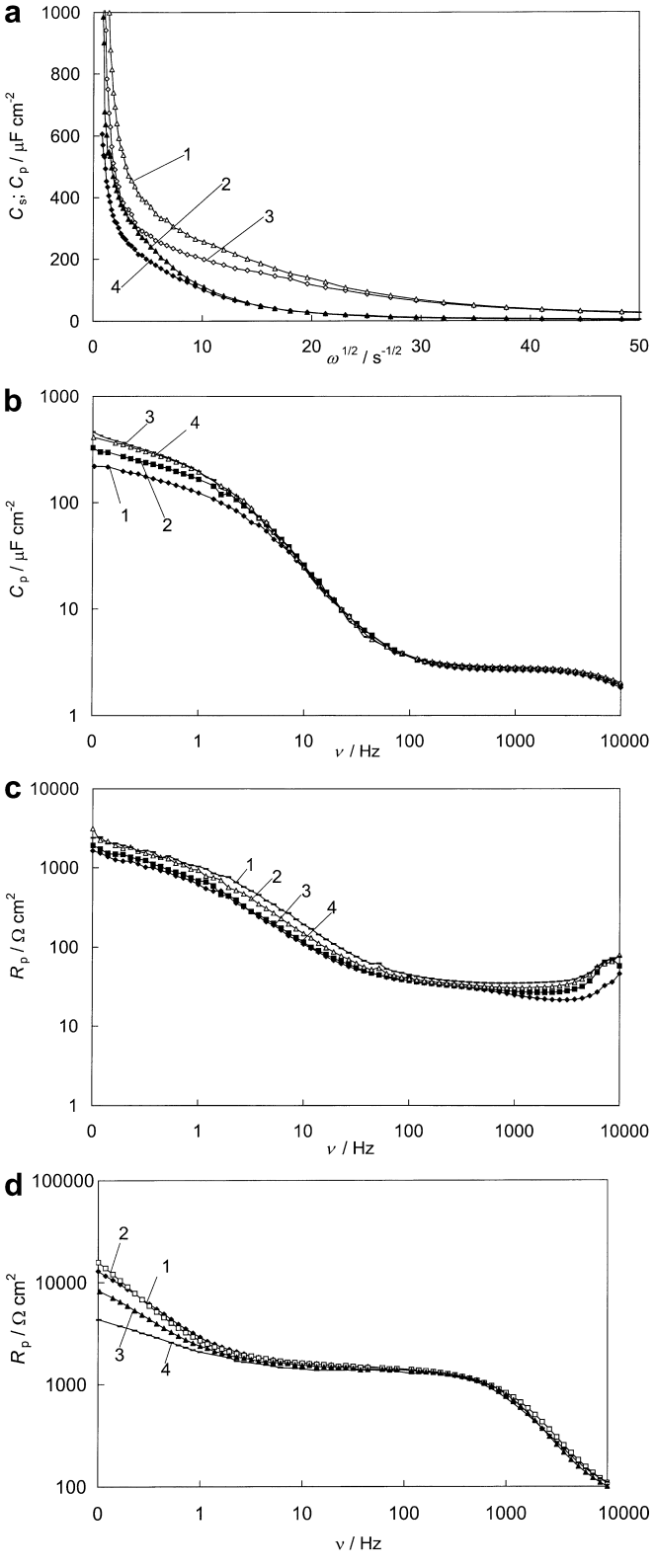

Fig. 8 **a** Dependence of C_s (*1*, *3*) and C_p (*2*, *4*) on $\omega^{1/2}$ [at electrode potentials (V): –0.4 (*1*, *2*) and 0.2 (*3*, *4*)]; **b** C_p and **c**, **d** R_p vs. a.c. frequency plots [at electrode potentials (V): 1.1 (*1*), 0.2 (*2*), –0.2 (*3*) and –0.4 (*4*)] for the DLCE|xM NaF + H_2O interface [$x = 0.1$ (**a**, **c**), 0.01 (**b**) and 0.001 (**d**)]

$\nu < 100$ Hz, a very high increase of C_s as well as C_p values takes place and thus very high capacitance values, compared with the smooth single-crystal metal electrodes, have been established at $\nu \approx 0.1$ Hz. Thus, at higher a.c. penetrability the DLCE surface demonstrates parameters that are characteristic for very rough (porous) electrodes. However, the values of C_s for the DLCE are $\sim 10^3$–10^5 times lower than for the NPCE [11]. The very weak dependence of C_s on E as well as the good agreement of C_s and C_p values in the region $-0.2 < E < 1.1$ V and the very high parallel resistance R_p values (Fig. 8c) indicate the absence of rapid faradaic processes at the DLCE|xM $NaF + H_2O$ interface. Comparison of Z', C_s, C_p, $|Z|$ and δ vs. logν dependences obtained at different electrolyte concentrations indicate that the solution phase characteristics (i.e. the electrolyte resistance, Debye screening length and diffuse layer capacitance) are very important parameters for obtaining the high-frequency characteristics (series resistance) of the DLCE|xM $NaF + H_2O$ interface. According to the data in Fig. 8c and d, the values of the parallel resistance R_p as well as the series resistance R_s noticeably decrease with the increase of the electrolyte concentration. The very high R_p values indicate that there is no rapid faradaic processes at $-0.3 < E < 1.0$ V.

Fitting the results of the experimental complex plane plots

Usually the Z'' vs. Z' plots, like those presented in Figs. 5a, 6a and 7a, have been simulated by the Randles-type equivalent circuit (circuit I in Fig. 9) that combines the high-frequency resistances of the electrode material and bulk electrolyte (R_{el}), the electrical double layer and adsorption capacitances (C_{dl} and C_{ad}), the ionic charge transfer resistance and double layer resistance (R_{ad}) at the front contact and the restricted diffusion (Warburg-like impedance, Z_W) of the adsorbed or inserted species (the insertion of cations Li^+ or H^+ as well as Na^+ cations in our case) into the electrode material from aqueous and non-aqueous solutions [44, 45, 46, 47, 48, 49, 50, 51, 52, 53]. In this case, the specific impedance and capacitance functions have the following forms:

$$Z(\omega) = R_{el} + \frac{1}{j\omega C_{dl} + \frac{1}{\frac{\sigma_{ad}}{\sqrt{j\omega}} + \frac{1}{j\omega C_{ad}} + R_{ad}}} \quad (1)$$

and

$$C(\omega) = \frac{1}{j\omega[Z(\omega) - R_{el}]} = C_{dl} + \frac{C_{ad}}{1 + \sigma_{ad} C_{ad} \sqrt{j\omega} + R_{ad} C_{ad} j\omega} \quad (2)$$

where $\sigma_{ad}(j\omega)^{-1/2}$ represents the diffusion (Warburg-like) impedance Z_W with its coefficient σ_{ad}. Studying the difference between the equivalent circuits presented in Fig. 9, there are two accurate ways to obtain an indication of how well the modelling function reproduces the experimental data set: (1) observing the parameter values and their relative error estimate (in %); (2) the chi-squared function (χ^2) also gives a good indication of the quality of the fit [43, 53, 54, 55, 56].

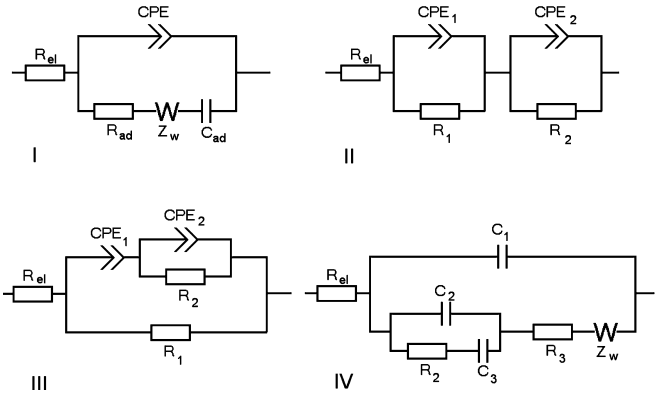

Fig. 9 Equivalent circuits used for fitting the experimental complex plane plots. *I*: combined Frumkin-Melik-Gaikazyan and Randles circuit, where CPE is the constant phase element, R_{ad} is the charge transfer resistance, Z_W is the Warburg-like diffusional impedance, and C_{ad} is the adsorption capacitance. *II*: circuit consisting of two CPE elements (CPE_1 and CPE_2) in parallel with the resistances R_1 and R_2 (see text). *III*: circuit in which R_{el} is the resistance of the electrolyte and DLCE material; CPE_1 is the constant phase element related to the capacitance of the Helmholtz layer and surface films; and CPE_2 is related to the capacitance of the flat electrode|electrolyte interface; R_1 is the charge transfer resistance of the flat electrode|solution interface; and R_2 is the partial charge transfer resistance at the internal surfaces of a rough electrode. *IV*: circuit in which R_{el} is the resistance of the electrode material and bulk electrolyte; Z_W is the Warburg-like impedance; C_1, C_2 and C_3 are the surface film, double layer and adsorption capacitances; and R_2 and R_3 are the charge (or partial charge) transfer and surface film resistances, respectively

The results of the fitting of our experimental Z'' vs. Z' plots (Fig. 10a), using the program Zview 2.2 for Windows (Scribner), shows that the agreement is not very good at smaller frequencies of $\nu < 5$ Hz ($\chi^2 \geq 1.5 \times 10^{-3}$ and the weighted sum of squares is $\Delta^2 \geq 0.14$) and therefore this simple model seems to be valid for the DLCE|xM $NaF + H_2O$ interface only to a first very rough approximation. The model of Ho et al. [54] is a modification of the Frumkin-Melik-Gaikazyan-Randles-type model and it predicts pure capacitive behaviour at low frequencies. However, in good agreement with the results of other studies [10, 11], the impedance is not purely capacitive for the DLCE|xM $NaF + H_2O$ interface at $\nu < 5$ Hz. Our results (Figs. 5, 6, 7, 10) show that a certain capacitance dispersion characteristic of polycrystalline solid electrodes has been observed and, in such cases, the impedance spectra (Z vs. ω) can be modelled by an equivalent circuit containing a constant phase element (CPE) showing power law frequency dependence:

$$Z_{CPE}(\omega) = A^{-1}(j\omega)^{-\alpha} \quad (3)$$

where ω is the angular frequency and $j = \sqrt{-1}$. According to the experimental results obtained for various metal electrodes, the smoother and cleaner the surface, the closer is the value of α to unity (at $\alpha = 1.0$, the value of the CPE coefficient A is equal to the capacitance of

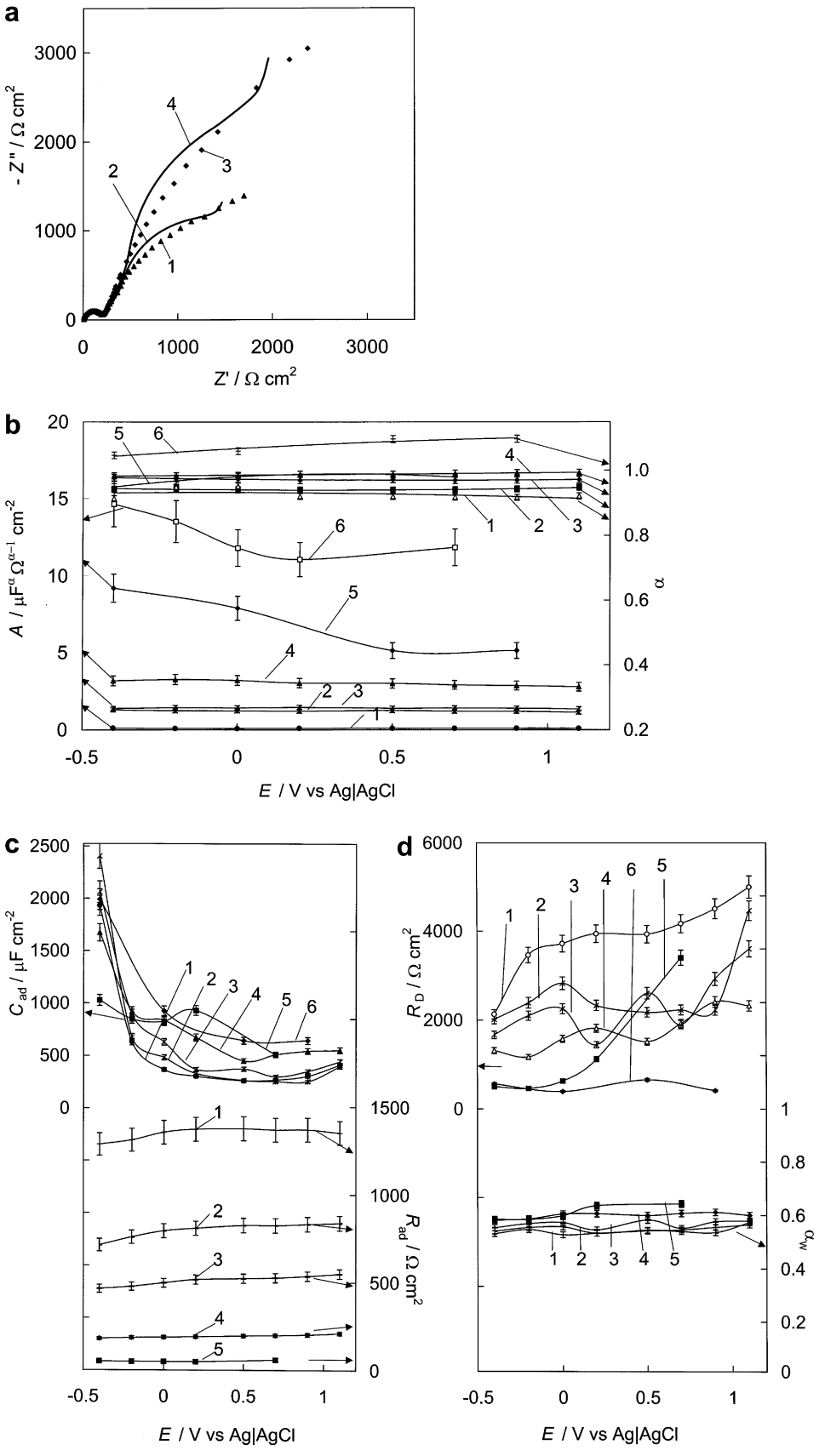

Fig. 10 **a** Experimental Z'' vs. Z' plots (*points*) (*1*, *3*) for the DLCE|0.01 M $NaF + H_2O$ interface and calculated curves according to the Frumkin-Melik-Gaikazyan and Randles model (*solid lines*) (*2*, *4*) at electrode potentials (V) of –0.4 (*1*, *2*) and 0.2 (*3*, *4*). **b** CPE coefficient A and fractional exponent α vs. electrode potential plots; **c** C_{ad} and R_{ad} vs. electrode potential plots; and **d** α_W and R_D vs. electrode potential plots for the DLCE|xM $NaF + H_2O$ interface with the following values of x: 0.001 (*1*), 0.002 (*2*), 0.003 (*3*), 0.01 (*4*), 0.05 (*5*) and 0.1 (*6*)

the double layer, but in the general case the frequency-independent constant A has the dimensionality $F^{\alpha}\ \Omega^{\alpha-1}\ cm^{-2}$). The dependences of A and α on E obtained for different electrolyte concentrations are given in Fig. 10b. The value of α somewhat decreases with dilution of the electrolyte, in the same direction as the constant A. The adsorption capacitance C_{ad} increases with c_{NaF} as well as with the negative polarization of the electrode, which can be explained by the more pronounced adsorption of Na^+ ions (and probably noticeable intercalation at $E \leq -0.4$ V) on the DLCE surface (Fig. 10c). This dependence is in good agreement with the decrease of the partial charge transfer resistance (or the "true" faradaic reaction resistance) (Fig. 10c) and diffusion resistance values (R_D) (Fig. 10d), obtained according to the generalized finite Warburg element (GFW) for a short circuit terminus model, expressed as:

$$Z_{GFW} = R_D \tanh[(jT\omega)^{\alpha_W}](jT\omega)^{-\alpha_W} \quad (4)$$

where R_D is the so-called limiting diffusion resistance; the so-called frequency parameter $T = L^2/D$, where L is the effective diffuse layer thickness and D is the effective diffusion coefficient of a particle; α_W is a fractional exponent, varying from 0 to 1. Values of α_W somewhat higher than 0.5 ($0.53 \leq \alpha_W \leq 0.63$) (Fig. 10d), as well as $T \neq 0$, indicate that there are small deviations of the DLCE|xM $NaF + H_2O$ interface from the classical semi-infinite diffusion layer model with $\alpha_W = 0.5$ [55, 56, 57, 58].

The analysis of the Z'' vs. Z' plots shows that the DLCE|xM $NaF + H_2O$ interface can be simulated with better accuracy by an equivalent circuit (circuit 2 in Fig. 9) which consists of two CPE elements (CPE_1 and CPE_2) in parallel with the resistances R_1 and R_2. According to the results of the fitting (Fig. 11a) ($\chi^2 \leq 1.3\times10^{-3}$ and $\Delta^2 \leq 0.1$), the first block of this circuit formally describes the electrical double layer (interfacial) parameters at low frequencies (i.e. mainly Helmholtz inner layer characteristics at rough internal surfaces of the DLCE) and the second parallel combination of CPE_2 and R_2 describes the high-frequency parameters of the DLCE|electrolyte interface, which seems "flat" at higher frequencies (at low a.c. penetration steps).

The results of the simulations show that there is a very well pronounced dependence of the values of A_1, A_2 (obtained from CPE_1 and CPE_2, respectively), R_1 and R_2 on the electrolyte concentration (Fig. 11b and c). For example, the parallel resistance of the so-called high-frequency part of the equivalent circuit (R_2) noticeably increases with the decrease of the electrolyte concentration, and the same is valid for A_2 and α_2 (obtained from CPE_2) according to Eq. 3. Except for A_2 values at higher electrolyte concentrations, the values of A_2, α_2 and R_2 are practically independent of the electrode potential and probably characterize the bulk electrolyte as well as the bulk electrode material characteristics. The value of A_2 noticeably decreases with the decrease of the electrolyte concentration and the very low values of A_2 for $c_{NaF} < 1\times10^{-2}$ M [10, 11], compared with metal electrodes, probably indicate the very large influence of the potential drop in the surface layer of the DLCE (i.e. the main potential drop is attributed to the space charge region within the DLCE) [59, 60, 61].

The values of A_1, related to CPE_1, are noticeably higher than A_2, which can be explained by the fact that the a.c. penetration depth is high at low frequencies and the whole surface of the rough DLCE participates actively in the electrical double layer formation process. The noticeable increase of A_1 with the negative polarization of the DLCE (Fig. 11b) can be explained by the weak adsorption of the Na^+ cations on the internal surface of the DLCE. The noticeably lower values of $\alpha_1 \leq 0.7$ compared with $\alpha_2 \geq 0.90$ indicate that the DLCE surface is geometrically inhomogeneous, as well as by the fact that the deviation of the system from purely capacitive behaviour ($\alpha = 1$) toward diffusion-limited behaviour ($\alpha = 0.5$) increases. Thus, the noticeable increase of A_1 and decrease of the parallel resistance R_1, as well as the fractional exponent α_1, probably indicate an increase in the rate of the partial charge transfer process (or "true" faradaic cathodic process resistance) with the negative polarization.

Taking into account the fact that there is a potential drop in the surface layer of the DLCE, the equivalent circuit III, presented in Fig. 9, has been used for fitting the experimental Z'' vs. Z' plots. In this circuit, R_{el} is the cell resistance, including the resistances of the bulk DLCE film and the bulk electrolyte solution; CPE_1 is the constant phase element related to the constant A_1 and α_1 (i.e. with capacitance C_1 if $\alpha_1 = 1.0$) corresponding to the elements (i.e. potential drops) which are located outside the semiconductor (e.g. to the various surface films and Helmholtz layer capacitance of the rough energetically and geometrically inhomogeneous surface of the DLCE, characterized by the fractional exponent α_1). In our case, CPE_2 is the frequency-independent element with the constant phase angle (characterized by A_2 and α_2) that describes the relaxation process occurring on the electrode surface and/or in the space charge region; R_2 is the resistance characterizing the charge transfer process at the (internal) electrode surface regions, i.e. the resistance of the intercalation process of cations (Na^+ and/or H^+ ions); R_1 is the parallel resistance for the "true" faradaic or partial charge transfer process at the macroscopically flat DLCE|solution interface. Analysis of the complex plane plots (Figs. 5, 6, 7) shows that the DLCE|xM $NaF + H_2O$ interface can be simulated with a good accuracy ($\chi^2 \leq 7\times10^{-4}$ and $\Delta^2 \leq 0.05$) (Fig. 12a) using the equivalent circuit III presented in Fig. 9. The parameters obtained from the fitting of the Z'' vs. Z' plots of the DLCE|xM $NaF + H_2O$ interface are given in Fig. 12b and c. According to these data, there is a noticeable dependence of R_1 and R_2 on the electrolyte concentration (Fig. 12b), as well as, for the more dilute electrolyte solutions, on the electrode potential. R_1 and R_2 increase noticeably with dilution of the electrolyte, but the values of R_1 are two orders higher than the R_2 values. The very

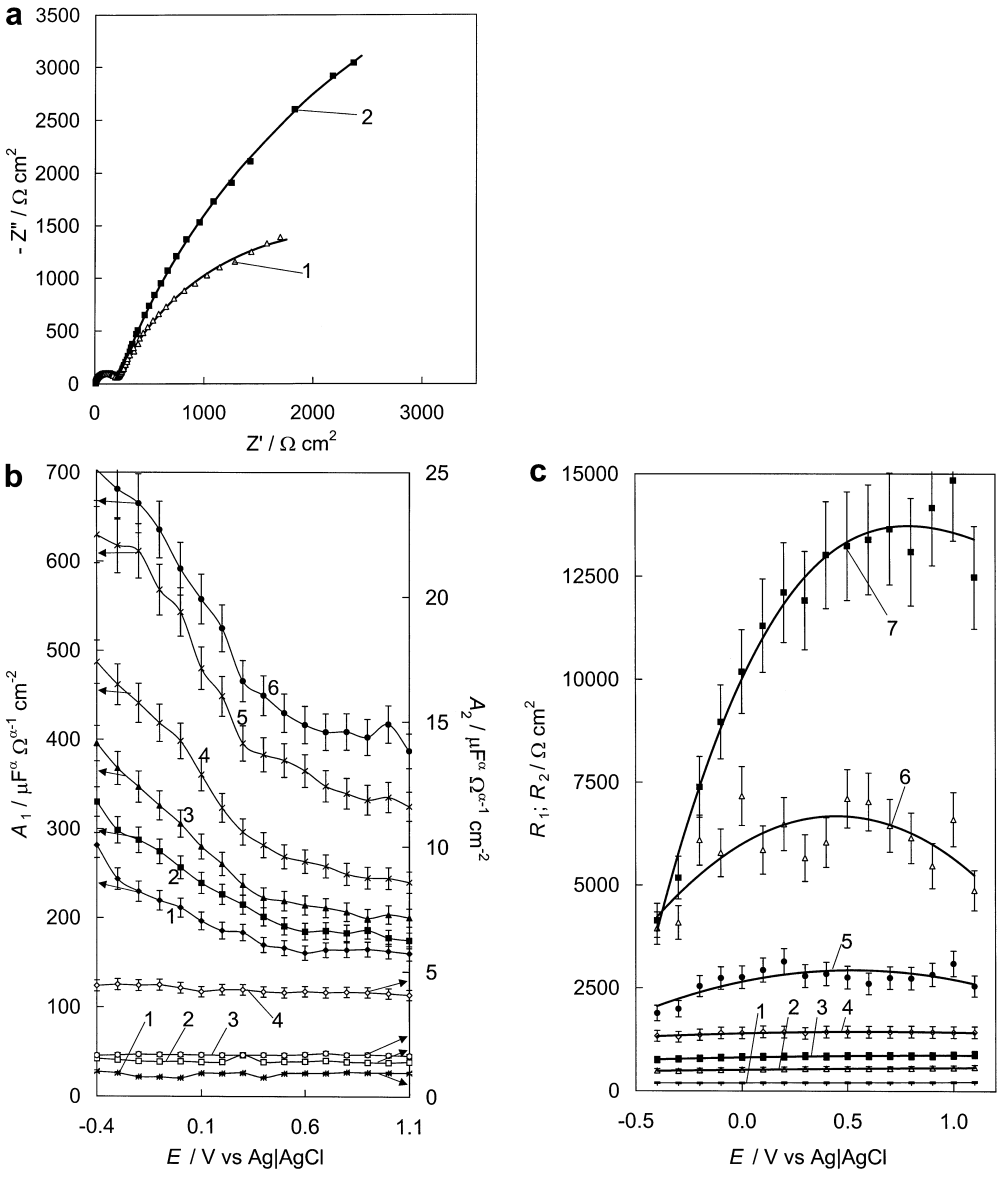

Fig. 11 **a** Experimental Z'' vs. Z' plots (*points*) for the DLCE|0.01 M $NaF + H_2O$ interface and calculated curves (*lines*) according to the equivalent circuit II in Fig. 9 (where CPE_1 and R_1 are the constant phase element and resistance, corresponding to the high-frequency region, and CPE_2 and R_2 characterize the low-frequency behavior of the system) at electrode potentials (V) of –0.4 (*1*) and 0.2 (*2*). **b** A_1 and A_2 and **c** and R_1 (*5–7*) and R_2 (*1–4*) versus electrode potential plots for the DLCE|*x*M $NaF + H_2O$ interface with the following values of *x* for **b**: 0.001 (*1*), 0.002 (*2*), 0.003 (*3*), 0.01 (*4*), 0.05 (*5*) and 0.1 (*6*); and for **c**: 0.01 (*1*), 0.003 (*2*), 0.002 (*3*), 0.001 (*4*), 0.1 (*5*), 0.05 (*6*) and 0.01 (*7*)

high R_1 values indicate that the influence of the parallel resistance R_1 (i.e. resistance of charge transfer or partial charge transfer on the macroscopically flat surface) is not important and, to a first very rough approximation, R_1 can be neglected in circuit III in Fig. 9. The noticeably lower values of α_1, compared with α_2, probably indicate the influence of the geometrical surface roughness and therefore the surface energetic inhomogeneity [i.e. dependence of the zero charge potential on various surface regions with different electronic states (sp^3 or sp^2 hybridization)] on the electrical double layer characteristics [i.e. interfacial Helmholtz and diffuse layer characteristics (capacitance, charge density), and capacitance and resistance parameters of various surface films, etc.] for the DLCE|*x*M $NaF + H_2O$ interface. The small decrease of α_1 with increasingly negative polarization can be explained by the increase of the rate of the faradaic (or partial charge transfer) reaction. The constant A_2 related to CPE_2 clearly depends on the electrolyte concentration and for a $c_{NaF} \geq 5 \times 10^{-2}$ M solution A_2 somewhat increases with the increase of the negative polarization of the DLCE. The values of A_1, related to CPE_1, are noticeably higher compared with the values of A_2, but the dependence of A_1 on c_{NaF} is more pronounced and, thus, the Helmholtz layer capacitance and/or capacitance of the surface films clearly depend on the surface charge density. This result is in good agreement with the lower values of α_1 (i.e. the fractional exponent of the Helmholtz layer and/or surface films) and its decrease with the increase of negative polarization. Thus, with the increase of the negative surface charge density, the deviation of the DLCE|*x*M $NaF + H_2O$ interface from the "flat" nearly ideally polarizable interface increases. Comparison of the values of A_1 with A_2 and R_1 with R_2 obtained using the equivalent circuits II and III shows that the influence of the resistance R_1 in circuit III on the other parameters obtained is very small at $0.1 < E < 1.1$ V

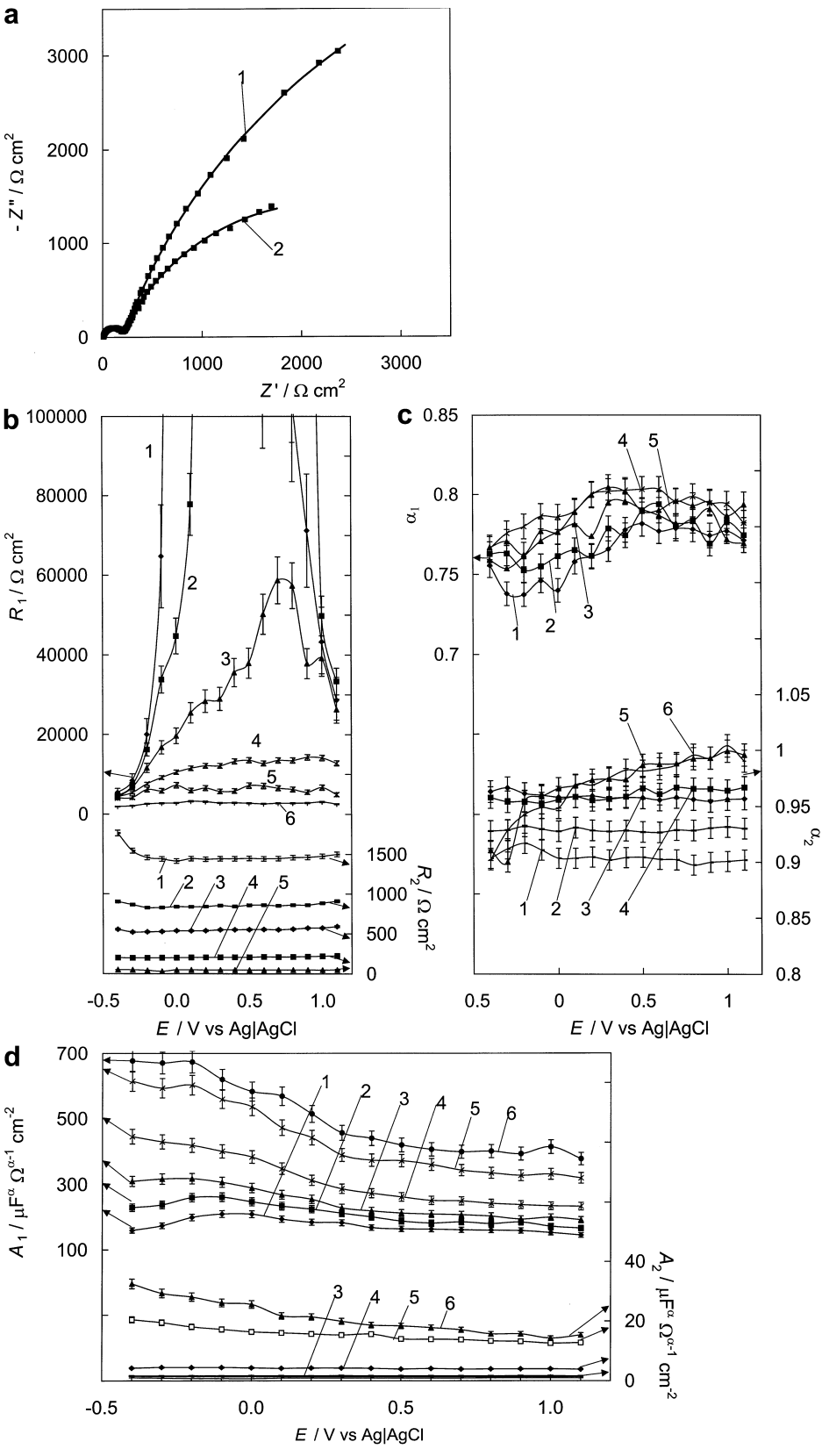

Fig. 12 **a** Experimental Z'' vs. Z' plots (*points*) for the DLCE|0.01 M $NaF + H_2O$ interface and curves calculated according to the equivalent circuit III (*lines*) at the following electrode potentials (V): 0.3 (*1*) and –0.3 (*2*). **b** R_1 and R_2, **c** α_1 and α_2 and **d** A_1 and A_2 vs. electrode potential plots for the DLCE|xM $NaF + H_2O$ interface with the following values of x: 0.001 (*1*), 0.002 (*2*), 0.003 (*3*), 0.01 (*4*), 0.05 (*5*) and 0.1 (*6*)

(because of the very high parallel resistance values) and therefore this equivalent circuit III can be simplified by neglecting the R_1 value. A good agreement between the A_1, A_2, α_1, α_2 and R_2 values obtained using circuits II and III gives some evidence that the values are quite realistic.

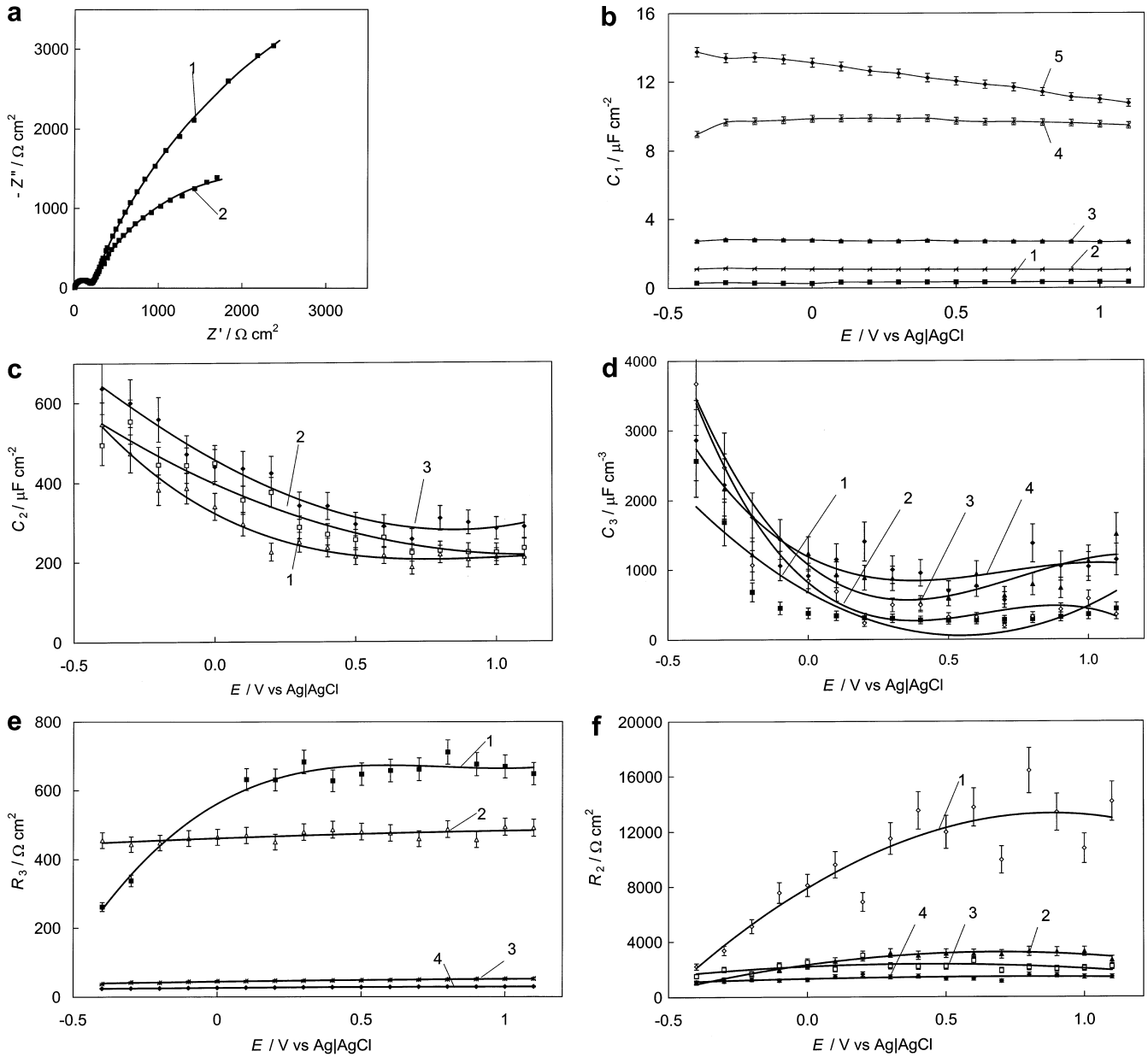

Fig. 13 **a** Experimental Z'' vs. Z' plots for the DLCE|0.01 M $NaF + H_2O$ interface (*points*) and curves (*solid lines*) calculated according to the equivalent circuit IV (in Fig. 9) at the following electrode potentials (V): 0.3 (*1*) and –0.3 (*2*). **b** C_1 vs. E curves [at the following values of x: 0.001 (*1*), 0.002 (*2*), 0.01 (*3*), 0.05 (*4*) and 0.1 (*5*)], **c** C_2 versus E plots [x: 0.003 (*1*), 0.05 (*2*) and 0.1 (*3*)], **d** C_3 vs. E curves [x: 0.001 (*1*), 0.003 (*2*), 0.01 (*3*), 0.05 (*4*) and 0.1 (*5*)], **e** R_3 vs. E curves [x: 0.001 (*1*), 0.003 (*2*), 0.05 (*3*) and 0.1 (*4*)], and **f** R_2 vs. E plots [x: 0.003 (*1*), 0.01 (*2*), 0.05 (*3*) and 0.1 (*4*)] for the DLCE|xM $NaF + H_2O$ interface

It should be noted that the excellent agreement between the simulations and the experimental data ($\chi^2 \leq 3\times10^{-4}$ and $\Delta^2 \leq 0.03$) for the DLCE|xM $NaF + H_2O$ interface has been established if circuit IV in Fig. 9 is used, in which the charge transfer and double layer charging at the surface, the intercalation of Na^+ or H^+ ions and solid phase diffusion inside the nanoparticle (i.e. in the nearly spherical particle; see AFM data in Fig. 3), as well as the effect of an insulating film at the surface (i.e. surrounding of the nanoparticles), have been taken into account [48, 49]. In this circuit, R_{el} is the series resistance, including the resistance of the bulk diamond film and bulk electrolyte solution; C_1 is the capacitance of the surface film, developed on the surface of the DLCE and described as a simple dielectric by Eq. 5:

$$C_1 = \varepsilon_f h_f^{-1} \tag{5}$$

where ϵ_f is the permittivity and h_f is the thickness of a diamond-like carbon film with resistance R_3. According to the results of the simulations, the capacitance of this film is comparatively small, but if the film is a dielectric, it is possible to separate the charge across it. Only at a very high frequency will there be a significant current flowing due to separation of charges across the film,

resulting in "shorting" the resistance of the film [49]. C_2 is the so-called interfacial (i.e. double layer) capacitance, which is caused by charging and discharging the electrical double layer at the internal surfaces of the rough electrodes; R_2 is the partial charge transfer or "true" faradaic reaction resistance of the film; C_3 is the adsorption capacitance; Z_W is the Warburg-like diffusional impedance, simulated using the Frumkin-Melik-Gaikazyan semi-infinite diffusion model ($\alpha_W = 0.5$) [57, 58] or by the generalized finite length Warburg short circuit model [55, 56].

The results of the simulations given in Fig. 13b–d indicate that the surface film capacitance C_1 is small in comparison with the "true" double layer capacitance C_2 and adsorption capacitance C_3. The high values of C_2 and C_3 are caused mainly by the very rough internal surface structure of the DLCE as well as by the weak adsorption of Na^+ ions, increasing with the increase of the negative surface charge density of the DLCE surface (Fig. 13c and d). The resistance of the surface film, R_3 (Fig. 13e), is smaller than corresponding values established by Meyers et al. [49] and therefore the conductivity of the surface films is higher. The partial charge transfer or "true " faradaic process resistance R_2 values are larger (Fig. 13f) compared with the results of Meyers et al. [49], and therefore the rate of the probable intercalation process of H^+ or Na^+ ions into the DLCE is smaller. The fitting results for the DLCE|xM $NaF + H_2O$ interface show that the so-called external impedance Z_{ext}, obtained by the parallel combination of external resistance R_{ext} and capacitance C_{ext} circuit elements [49], has to be replaced by the Warburg-like diffusional impedance Z_W, calculated according to Eq. 4. The fitting data show that the diffusional resistance R_D (Fig. 14a) decreases with the increase of electrolyte concentration as well as of the negative polarization. The values of the fractional exponent α_W in Eq. 4 are very close to 0.5 (Fig. 14b) and, to a first approximation, the classical semi-infinite diffusion layer model seems to be applicable for the DLCE|xM $NaF + H_2O$ interface.

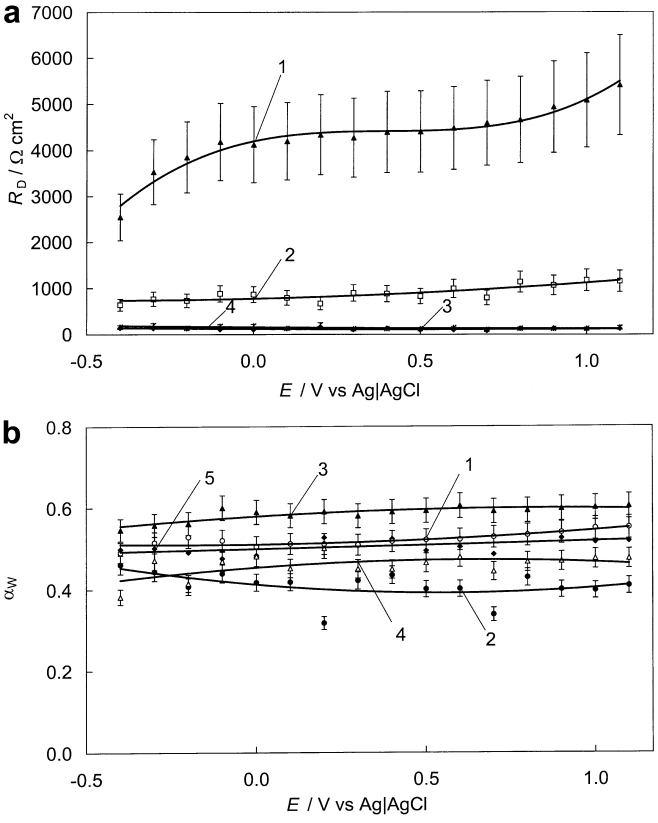

Fig. 14 **a** R_D vs. E plots [x: 0.001 (*1*), 0.003 (*2*), 0.05 (*3*) and 0.1 (*4*)] and **b** α_W vs. E plots [x: 0.001 (*1*), 0.003 (*2*), 0.01 (*3*), 0.05 (*4*) and 0.1 (*5*)] for the DLCE|xM $NaF + H_2O$ interface

Conclusions

The cyclic voltammetry and impedance data for the DLCE|xM $NaF + H_2O$ interface show that this system is nearly ideally polarizable in the potential region $-0.4 < E < 1.1$ V [vs. AgCl|Ag (sat. KCl in H_2O)]. The root-mean-square roughness is $R_{ms} \geq 81$ Å (established by AFM) and the medium size of a DLCE particle is about 0.1 μm. The shape of complex plane plots depends on the electrode potential and noticeably on the electrolyte concentration. The non-linear least squares fitting method of the experimental data shows that various equivalent circuits can be used for fitting the experimental complex plane plots, but an excellent fit has been established using a circuit combining the total resistance R_{el} of the electrode system, including the resistance of the bulk diamond film and bulk electrolyte solution, the capacitance C_1 and the resistance R_3 of the surface film, developed on the surface of the DLCE, the so-called interfacial (i.e. double layer) capacitance C_2 (caused by the charging and discharging of the electrical double layer at the internal surface of DLCE), the partial or "true" faradaic reaction resistance of the film R_2, the adsorption capacitance C_3 and the Warburg diffusion impedance Z_W.

The distributed nature of the impedance (at low frequency) results in just an engagement of the available surface area. Rather than passing current through only a single particle, current passes through all of the particles in the rough or porous electrode without any noticeable additional ohmic drop. The ohmic drop in the solution phase (for the systems simulated) greatly affects the overall impedance of the rough (porous) electrode, increasing its magnitude and decreasing its phase angle (Figs. 5, 6, 7) [10, 11, 48, 49]. It is clear that the breadth of the particle-size distribution affects the solid-phase diffusion impedance, except in its high-frequency limit. The low-frequency limit yields no useful information about the diffusion coefficient in the solid unless the particle-size distribution is well known [49].

Acknowledgements This work was supported partially by the Estonian Science Foundation under project nos. 4568 and 4204.

References

1. Pleskov YuV, Sakharova AYa, Krotova MD, Bouilov LL, Spitsyn BV (1987) J Electroanal Chem 228:19
2. Pleskov YuV, Evstefeeva YuE, Krotova MD, Elkin VV, Mazin VM, Mishuk VYa, Varin VP, Teremetskaya IG (1998) J Electroanal Chem 455:139
3. Janssen G, van Enckevort WJP, Wollenberg W, Giling LJ (1992) Diamond Relat Mater 1:789
4. Ball P (1996) Nature 381:116
5. van de Lagenmaat J, Vanmaekelbergh D, Valley JJ (1999) J Electroanal Chem 475:139
6. Tenne R, Patel K, Hashimoto K, Fujishima A (1993) J Electroanal Chem 347:409
7. Vinokur N, Miller B, Avyigal Y, Kalish R (1996) J Electrochem Soc 143:L238
8. Alhashem S, Chambers F, Stojek JW, Swain GM, Ramesham R (1995) Anal Chem 67:2812
9. Martin HB, Argoitia A, Landau U, Anderson AB, Angus JC (1996) J Electrochem Soc 144:L133
10. Conway BE (1999) Electrochemical supercapacitors: scientific fundamentals and technological applications. Kluwer/Plenum, New York, p 1
11. Lust E, Nurk G, Jänes A, Arulepp M, Nigu P, Permann L, Möller P (2002) J Condens Matter Phys 2:1
12. Swain GM (1994) Adv Mater 6:388
13. Pleskov YuV, Mishuk VYa, Abaturov MA, Elkin VV, Krotova MD, Varin VP, Teremetskaya IG (1995) J Electroanal Chem 396:227
14. Pleskov YuV, Elkin VV, Abaturov MA, Krotova MD, Mishuk VYa, Varin VP, Teremetskaya IG (1996) J Electroanal Chem 413:105
15. Sakharova AYa, Pleskov YuV, Quarto FD, Piazza S, Sunseri C, Teremetskaya IG, Varin VP (1995) Russ J Electrochem 31:169
16. Sakharova AYa, Sevastyanov AE, Pleskov YuV, Teplitskaya GL, Surikov VV, Voloshin AA (1991) Elektrokhimiya 27:263
17. Kulish W (1999) Deposition of diamond-like superhard materials. Springer, Berlin Heidelberg New York, pp 1–186
18. Tabal M, Mérel P, Chaker M, El Khakani MA, Herbert EG, Lucas MB, O'Hern ME (1999) Surf Coating Technol 116:452
19. Tsui YY, Redmon DG (2000) Surf Coat Technol 126:96
20. Wei Q, Samkar J, Sharma AK, Yamagata Y, Narayan J (2001) J Vacuum Sci Technol A 19:311
21. Ebihara K, Nakamiya T, Ohshima T, Ikegami T, Aoqui S (2001) Diamond Relat Mater 10:900
22. Okada K, Aizawa T, Souda R, Komatsu S, Matsumoto S (2001) Diamond Relat Mater 10:1991
23. Wei Q, Sankar J, Nakayan J (2001) Surf Coat Technol 146–147:250
24. Tomcik B, Seng SC, Balakoisnan B, Lee J Y (2002) Diamond Relat Mater 11:1409
25. Robertson J (2002) Mater Sci Eng Res Rep 37:129
26. Gao J (2002) Int Mod Phys B 16:1024
27. Fedosenko S, Korzec D, Engemann J, Lyebyedyev D, Scheer H-C (2002) Thin Solid Films 406:275
28. Ferrari A C (2002) Diamond Relat Mater 11:1053
29. Zhang S, Hing P, Gao J (2002) Diamond Relat Mater 11:160
30. Rao TN, Tryk DA, Hashimoto K, Fujishima A (1999) J Electrochem Soc 196:680
31. Yagi I, Tsunosaki K, Tryk DA, Fujishima A (1999) Electrochem Solid State Lett 2:457
32. Jantson T, Avarmaa T, Mändar H, Eskusson J, Lõhmus A, Jaaniso R (2001) Proc SPIE 4318:36
33. Xiao RF (1995) Appl Phys Lett 67:1022
34. Xiao RF (1995) Appl Phys Lett 67:3117
35. Nurk G, Jänes A, Lust K, Lust E (2001) J Electroanal Chem 515:17
36. Lust E, Jänes A, Sammelselg V, Miidla P, Lust K (1998) Electrochim Acta 43:373
37. Lust E, Jänes A, Sammelselg V, Miidla P (2000) Electrochim Acta 46:185
38. Lust E, Jänes A, Lust K, Sammelselg V, Miidla P (1997) Electrochim Acta 42:2861
39. Leppävuori S, Levoska J, Vaara J, Kusmartseva O (1993) Mater Res Soc Symp Proc 285:557
40. Apakina VN, Karuzskii AL, Kogan MS, Kvit AV, Melnik NN, Mityagin YuA, Murzin VN, Orlikovsky AA, Perestoronin AV, Tkachenko SD, Volchkov NA (1997) Diamond Relat Mater 6:564
41. Knight DS, White WB (1989) J Mater Res 4:385
42. Diamant R, Jimenez E, Haro-Poniatowski E, Ponce L, Fernandez-Guasti M, Alonso JC (1999) Diamond Relat Mater 8:1277
43. MacDonald JR (1987) Impedance spectroscopy: emphasizing solid materials and systems. Wiley, New York
44. de Levie R (1990) J Electroanal Chem 281:1
45. MacDonald JR (1989) Solid State Ionics 13:147
46. Nyikos L, Pajkossy T (1986) Electrochim Acta 31:1347
47. Liu P, Wu H (1996) Solid State Ionics 92:91
48. Doyle M, Meyers JP, Newman J (2000) J Electrochem Soc 147:99
49. Meyers JP, Doyle M, Darling RM, Newman J (2000) J Electrochem Soc 147:293
50. Rammelt U, Reinhard G, Rammelt K (1984) J Electroanal Chem 180:327
51. Tanguy J, Mermilliod N, Hoclet M (1987) J Electrochem Soc 134:795
52. Paasch G, Micka K, Schwarzenberg M, Jobst K, Sawtschenko L (1992) Electrochim Acta 37:2453
53. Paasch G, Micka K, Gersdorf P (1993) Electrochim Acta 38:2653
54. Ho C, Raistrick D, Huggins R (1980) J Electrochem Soc 137:343
55. MacDonald JR (1992) Ann Biomed Eng 20:289
56. Jacobsen T, West K (1995) Electrochim Acta 40:233
57. Frumkin AN, Melik-Gaikazyan VI (1951) Dokl Akad Nauk SSSR 77:855
58. Melik-Gaikazyan VI (1952) Zh Fiz Khim 26:560
59. Randin J-P, Yeager E (1972) J Electroanal Chem 36:257
60. Gerisher H (1985) J Phys Chem 89:4249
61. Gerisher H, McInture R, Sherson D, Strock W (1987) J Phys Chem 91:1930
62. Daikhin LI, Kornyshev AA, Urbakh M (1997) Electrochim Acta 42:2853
63. Daikhin LI, Kornyshev AA, Urbakh M (1998) J Chem Phys 108:171